Environmental Science Nano

ROYAL SOCIETY OF CHEMISTRY

PAPER

View Article Online
View Journal

Cite this: DOI: 10.1039/d5en01203a

Photochemically facilitated todorokite nanoparticle formation in circumneutral pH environments

Haesung Jung, †[ab] Zhenwei Gao †[a] and Young-Shin Jun *[a]

Received 26th December 2025,
Accepted 3rd March 2026

DOI: 10.1039/d5en01203a

rsc.li/es-nano

The formation of Mn oxides and their reactivities affect electron flows and important redox-sensitive element cycles in nature. Thus, understanding the formation of nano-Mn oxides provides critical information about Earth's redox systems. Natural Mn oxides mostly occur with both layered and large tunneled (todorokite) nanostructures. However, while biotic/abiotic processes well explain how the layered structures form, the widespread occurrence of tunneled todorokite nanomaterials in nature remains puzzling owing to the difficulty in reproducing their formation under environmentally relevant conditions. Here, we show that todorokite forms directly *via* the oxidation of Mn^{2+}(aq) by superoxide generated from photochemical reactions under circumneutral aqueous conditions. We also explore that Mn(III) plays a key role by accommodating $Mg(OH)^{+}$ through charge compensation, with $Mg(OH)^{+}$ acting as a framework unit in the formation of nanoscale todorokite. This study suggests a new paradigm for the homogeneous formation of todorokite, which has been hitherto believed to be a secondary mineral phase resulting from diagenesis of layer-structured Mn oxides, under environmentally relevant conditions. In addition, our findings suggest a sustainable and facile pathway for the synthesis of todorokite nanostructures with potential applications in energy storage and catalysis.

Environmental significance

Natural nanostructured Mn oxides play a pivotal role in controlling environmental redox processes, with their nanoscale crystalline structures strongly governing the redox reactivity. However, the origin of various crystalline structures of Mn oxides remains elusive. This study reveals a new mechanism for the homogeneous formation of todorokite (a tunnel-structured MnO_2) *via* abiotic oxidation of Mn^{2+}(aq). Our findings challenge the longstanding view that todorokite forms only through slow, high-temperature transformations of layer-structured Mn oxides. This report shows that todorokite nanostructure can form directly at circumneutral pH, suggesting a potential pathway that explains its widespread occurrence in various environments. This insight has implications for more accurately predicting the fate and transport of Mn oxides and their reactivities towards contaminants in environmental systems.

Introduction

The manganese oxidation states (Mn(II), Mn(III), and Mn(IV)) play critical roles in redox cycles of natural elements, organics, and heavy metals in environmental systems.[1–4] Together with the profound roles of Mn redox cycles in carbon cycles and photosynthesis, the fundamental understanding of electron and energy flow of Mn oxide nanomaterials has received highlights in environmental chemistry and energy applications.[5–8] In addition, thanks to the high reduction potential of Mn (~500 mV, $Mn^{2+}/Mn(IV)O_2$), natural nano-Mn oxides can provide valuable evidence about planetary environmental conditions, such as the presence of oxygen on early Earth and Mars.[9,10] For these reasons, gaining a deeper understanding of the formation of Mn oxide nanostructures can not only shed light on the redox chemistry in environmental systems but also facilitate the design of engineered Mn oxides with tailored redox properties.

In nature, Mn(III/IV) oxides form through the oxidation of Mn^{2+}(aq). Previous studies investigated the abiotic homogeneous oxidation of Mn^{2+}(aq) by dissolved O_2 under circumneutral pH conditions in the dark to explain the ubiquitous formation of Mn oxides in environmental aqueous systems.[11–14] The studies showed that $Mn(OH)_2$(aq) serves as the key reactive species controlling oxidation kinetics in the dark. For the abiotic heterogeneous oxidation of Mn^{2+}(aq) by dissolved O_2 in the dark, previous work examined bidentate complexation of Mn^{2+}(aq) on the surface of minerals, such as iron oxides, aluminum oxides, *etc.*[11–13]

[a] *Department of Energy, Environmental and Chemical Engineering, Washington University, St. Louis, Missouri, 63130, USA. E-mail: ysjun@seas.wustl.edu; Fax: +(314)935 7211; Tel: +(314)935 4539; Web: http://encl.engineering.wustl.edu/*
[b] *Department of Chemical Engineering, Changwon National University, Changwon-si, Gyeongsangnam-do, 51140, Republic of Korea*
† These authors contributed equally to this work.

However, both abiotic homogeneous and heterogeneous oxidations of Mn^{2+}(aq) are typically sluggish reactions compared to biotic processes.[2,10,11,15–18] Preceding studies estimated the relative rates of abiotic homogeneous, abiotic heterogeneous (surface-catalyzed), and biotic oxidation of Mn^{2+}(aq) in representative natural waters to be on the order of 1 : 10 : 1000.[2,12] Furthermore, the oxidation rate of Mn^{2+}(aq) in natural waters is similar to that of biotic processes.[15] From the observed fast biotic oxidation of Mn^{2+}(aq) and its ubiquity in natural systems,[19] biotic processes have often been believed to be the dominant contributors to the formation of natural Mn oxide nanomaterials. Interestingly, recent studies have revealed a new mechanism of the rapid oxidation of Mn^{2+}(aq) *via* reaction with superoxide ($O_2^{\bullet-}$), which is generated through abiotic photochemical or extracellular biotic processes.[17,20–23] The studies further demonstrated that abiotic oxidation of Mn^{2+}(aq) to Mn(IV) by superoxide occurs under environmentally relevant conditions. Given the ubiquitous presence of superoxide in terrestrial and marine systems,[24,25] the equally abundant abiotic oxidation of Mn^{2+}(aq) in nature can be more important than we have considered in elucidating the formation of natural Mn oxides and the electron discharge of natural Mn oxides to maintain redox reactivity in nature.[17,20,21,26]

Previous reports on the fast oxidation of Mn^{2+}(aq) by biotic processes or superoxide have shown only the formation of layer-structured nano-Mn oxides (*i.e.*, phyllomanganate).[2,21,27] In natural systems, however, todorokite (*i.e.*, a tunnel-structured Mn oxide, tectomanganate) is as common as layer-structured Mn oxides.[28] Todorokite's large tunnels incorporate a wide variety of elements, including alkalis, transition metals, and rare earth metals,[29] and its unique structure is of interest in environmental remediation and energy applications.[30,31] The formation of todorokite in solution has not been well elucidated in environmentally relevant systems. The most widely investigated pathway for the formation of todorokite has been *via* the phase transformation of layered Mn oxides.[29,32–34] Moreover, the phase transformation of layer-structured Mn oxides to todorokite in laboratory systems has been achieved mostly under elevated temperature conditions or with pH values outside circumneutral conditions, which are far from natural environments.[29,32–34] Considering that todorokite is found ubiquitously under natural low temperature conditions, such as in deep sea Mn nodules and the oxidized zone of terrestrial Mn deposits,[28] the widespread occurrence of todorokite remains an outstanding puzzle in geoscience and environmental science. Lately, using an electrochemically driven process, Jung *et al.* (2020) showed transformation of layered Mn oxide to todorokite under room temperature and neutral pH conditions.[8] Even so, because this result still reflects a phase transformation pathway and provides limited insight into direct formation mechanisms, it remains unclear whether todorokite formation in nature occurs exclusively through phase transformation or can also proceed *via* direct formation during the oxidation of Mn^{2+}(aq).

Studies have explored the direct formation of todorokite through the oxidation of Mn^{2+}(aq) on engineered materials. Heo *et al.* (2025) reported the heterogeneous formation of todorokite on fluorine-doped tin oxide (FTO) *via* electrodeposition at pH values above 8.[35] Nevertheless, this electrochemical approach cannot be directly applicable to explain todorokite formation in natural environments. On the other hand, Jung *et al.* (2021) demonstrated the heterogeneous formation of todorokite on TiO_2 through photocatalytic oxidation of Mn^{2+}(aq) by superoxide, but this process is still representative of engineered systems rather than natural environmental conditions.[36] To examine more environmentally relevant conditions, Gao *et al.* (2025) studied photochemically induced oxidation of Mn^{2+}(aq) to form todorokite in high initial pH solution.[37] In that study, the solution pH was not strictly controlled and gradually decreased from pH 9 to pH 6, as the addition of pH buffer would have interfered with Mn^{2+}(aq) oxidation and altered Mn oxide speciation. To further assess the environmental relevance and ubiquity of todorokite formation, a systematic investigation under circumneutral pH conditions (between 7 and 8) is necessary.

To address the knowledge gaps discussed above, in this study, we examined the direct homogeneous formation of todorokite nanostructures through the oxidation of Mn^{2+}(aq) under the environmentally relevant conditions. Unlike our prior work, this novel formation pathway occurs at circumneutral pH (between 7 and 8) maintained by manual titration in the presence of Mg^{2+}, a common cation in natural and synthetic todorokite nanomaterials that occupies the tunnels as a large hydrated cation.[28,38,39] In what follows, we analyze this newly revealed todorokite formation mechanism in detail and discuss its possible occurrence in environmental systems. We employ a comprehensive characterization suite, including synchrotron based X-ray absorption spectroscopy (XAS) and X-ray diffraction (XRD) data, to identify detailed todorokite nanostructures. This study complements our earlier high pH work by revealing a distinct, circumneutral pH formation route driven by photochemically generated reactive oxygen species.

Materials and methods

Materials and solution preparation

Chemicals used in this study were at least American Chemical Society grade. Experimental solutions for all conditions were prepared with 100 μM $MnCl_2$ (Beantown Chemical) and 1 mM $NaNO_3$ (J.T. Baker), representing freshwater conditions. In addition to freshwater conditions, we also investigated saline water conditions. To mimic the oxidation of Mn^{2+}(aq) in seawater, 500 mM NaCl (VWR Chemicals BDH), 50 mM $MgCl_2$, and 10 mM $CaCl_2$ were added. All chemicals were dissolved in deionized water (resistivity ≥ 18.2 ΩM cm). To investigate the effect of pH on the formation of Mn oxides, two different pH programs were tested: either the pH was adjusted to between 7 and 8 every

30 min, or an initial pH 6 was used, without further pH adjustment. To clarify the effect of aqueous species on the formation of todorokite, a control experiment was conducted at an initially adjusted pH value of 9, using 10 mM NaOH, without further pH adjustment during the photochemical oxidation. The experiments at initially adjusted pH value of 6 or 9 show pH drops through the photochemical reaction (Fig. S1). Because of potential issues arising from adding a pH buffer chemical, such as ion or surface complexation, buffer chemicals were not applied in this study. Instead, during pH adjustments, 10 mM NaOH was slowly added dropwise, and the solutions were vigorously mixed by a magnetic stir bar. To study the effect of Mg^{2+} on the formation of Mn oxides, 1, 10, or 100 mM $MgCl_2$ (VWR Chemicals BDH) was added to the solution. To isolate the role of Mg^{2+}, control experiments were conducted by replacing Mg^{2+} with Na^+. Instead of $MgCl_2$, 1 or 100 mM NaCl (Sigma Aldrich) was added to the solution at pH 7–8. The thermodynamic equilibrium of Mg^{2+} in solutions was calculated using Visual MINTEQ and the 'thermo.vdb' database. The equilibrium concentration of Mn(II) in comproportionation was obtained based on an equilibrium constant value of $10^{-7.01}$, as suggested in experimental studies of the formation of manganite (γ-Mn(III)OOH) *via* comproportionation.[40,41]

Superoxide-mediated oxidation of Mn^{2+}(aq) and the formation of Mn oxides

Nitrate photolysis was used to generate superoxide for oxidizing Mn^{2+}(aq) to Mn(IV) and subsequently forming Mn oxides, using a 450 W Xe-arc lamp (Newport 6279NS) equipped with a water optical filter to remove infrared light and maintain a controlled reaction temperature.[21,22,42–44] The experiment solutions were contained in a cylindrical glass reactor with a quartz window facing the light source. After 6 h of reaction, the synthesized solid products were collected by centrifugation at 10 000 rpm for 30 min. To remove any residual traces of the liquid supernatant, the collected solid products were sequentially washed in DI water and centrifuged at 5000 rpm for 5 min: this process was repeated five times. The resulting solid products were dried at room temperature for further characterization. The oxidation rate was obtained by colorimetry using leucoberbelin blue (LBB).[21,45] Due to the difficulty arising from the mixed oxidation states of Mn oxides, we used $KMn(VII)O_4$ to calibrate the LBB colorimetry and then calculated the Mn(IV) equivalent concentration.[45]

Mn oxides solid phase characterization

High-resolution X-ray diffraction (HRXRD, using a Bruker D8 Advance X-ray diffractometer with Cu Kα radiation (λ = 1.5418 Å)) identified the mineral phase of Mn oxide samples. The Mn oxidation state and the existence of Ca or Mg in the Mn oxide samples were identified by X-ray photoelectron spectroscopy (XPS), using a PHI 5000 VersaProbe II, UlvacPHI with monochromatic Al Kα radiation (1486.6 eV). The C 1s peak (284.8 eV) was the reference peak, and asymmetric fitting using MultiPak provided the ratio of Mn(II), Mn(III), and Mn(IV). Because Mn 2p is less sensitive to the bonding environment of Mn oxides and Mn 3s overlaps Mg 1s, we used the highly sensitive Mn 3p peak in analyses of the oxidation state of Mn.[46] As reference materials, we selected β-Mn(IV)O_2, γ-Mn(III)OOH, and Mn(II)O (Fig. S2). The morphology and phases of Mn oxides were characterized by high-resolution transmission electron microscopy (HR-TEM), using a JEOL-2100F. The Mn oxides solid products were first sonicated for about 15 min to disperse them well. Then a droplet of the suspension was placed on an ultrathin lacey carbon film coated-Cu grid (LC400-Cu-UL, Electron Microscopy Science, PA) for imaging. Lattice fringes were obtained to identify the phases of Mn oxides. For XAS, the Mn K-edge was measured in transmission mode on beamline 7D at the Pohang Accelerator Laboratory in South Korea. Two sets of Si(111) crystals, giving a focused beam size of 1 mm by 2 mm and a resolution of 2×10^{-4} $\Delta E/E$, were used to create monochromatic X-ray. The energy flux was 2×10^{11} at 10 keV, and the energy range for this station was 5–21 keV. Energy calibration was monitored by using the pre-edge feature of Mn metal foil (6539.0 eV). The reference spectra of extended X-ray absorption fine structure (EXAFS) of todorokite, asbolane, and δ-MnO_2 were obtained from data deposited at Harvard Dataverse.[47]

Results

Rapid formation of todorokite nanostructures

In our experiments, todorokite nanomaterials formed rapidly through the oxidation of Mn^{2+}(aq) by photochemically generated superoxide in the presence of Mg^{2+}. Importantly, the nanoscale formation occurred even under circumneutral pH (between 7 and 8) conditions at room temperature, which has never previously been considered feasible (Fig. 1). X-ray diffraction (XRD) clearly showed diffractions at ~10, ~5, and ~3.3 Å, a pattern manifested only by todorokite, buserite and asbolane among more than 30 different Mn oxide polymorphs (Fig. 1A). Buserite, which has an expanded layered structure of birnessite due to hydration, also has similar diffractions at ~10 and ~5 Å, coming from the (001) and (002) basal planes, respectively. Buserite, a hydrated form of layered birnessite, shows similar reflections at ~10 and ~5 Å that originate from the (001) and (002) basal planes, respectively. However, buserite is structurally unstable upon drying. Because interlayer water is readily removed during sample preparation for XRD, particularly under drying at 100 °C, buserite undergoes collapse of the interlayer spacing.[48] This dehydration results in birnessite-like reflections at ~7.2 and ~3.6 Å, corresponding to the (001) and (002) basal planes. The absence of these dehydrated basal reflections after drying therefore suggests that buserite is not the predominant Mn oxide phase. Hereafter, we use 'birnessite' to express layer-structured Mn oxides (*i.e.*, birnessite and δ-MnO_2).[49] Notably, the

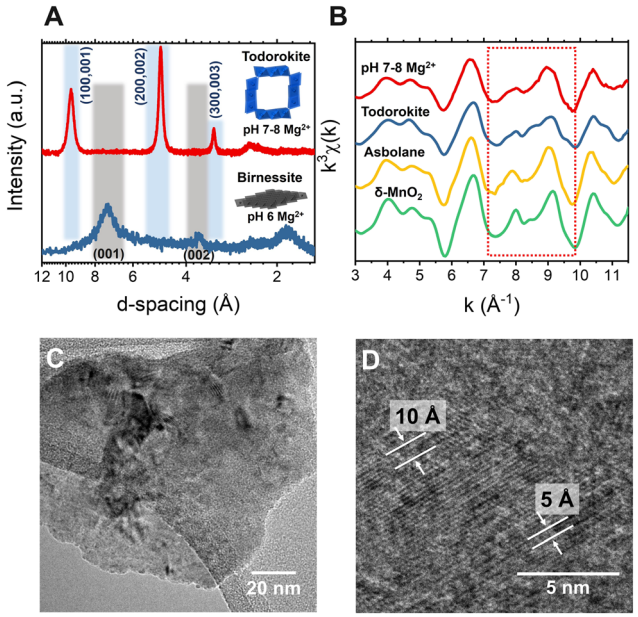

Fig. 1 The formation of todorokite at pH 7–8 in the presence of Mg^{2+}. (A) X-ray diffraction of Mn oxides shows the clear diffractions of todorokite (blue bar) at pH 7–8. At pH 6, only birnessite (or δ-MnO_2) was observed after 6 h reaction. (B) The analysis of extended X-ray absorption fine structure supports the formation of todorokite at pH 7–8. TEM images of the platy show the morphology of poorly crystalline todorokite (C) and the large *d*-spacing of todorokite (D) prepared at 100 mM Mg^{2+} pH 7–8.

diffraction patterns remained unchanged even after drying at 100 °C for 1 day (Fig. S3), which is inconsistent with the expected dehydration behavior of buserite. Asbolane, a phyllomanganate with an incomplete $Me(OH)_2$ (*e.g.*, $Ni(OH)_2$) octahedral layer in its interlayers, also exhibits reflections at approximately 10 Å, 5 Å, and 3.3 Å. While the (002) reflection in asbolane exhibits stronger diffraction compared to the (001) reflection,[50] our result showed that the stronger diffraction at around 10 Å relative to 5 Å only occurred after a longer reaction time of 12 hours (Fig. S3). To robustly distinguish among todorokite, buserite, and asbolane, we further analyzed the synthesized Mn oxides using extended X-ray absorption fine structure (EXAFS) spectroscopy (Fig. 1B and S4). Todorokite and layer-structured Mn oxides have significant differences in the region between 8 and 9.5 $Å^{-1}$, known as indicator region (boxed in Fig. 1B).[49,51–54] The obtained EXAFS spectrum of the synthesized Mn oxide in this study showed less sharp and broader peaks at ~8 and ~9.2 $Å^{-1}$ than that of the references of layer-structured Mn oxides (*i.e.*, asbolane and δ-MnO_2) (Fig. 1B and S4). In addition, the steadily rising slope from 8 to 9.2 $Å^{-1}$ is also a feature of todorokite, as shown in the EXAFS spectra of reference Mn oxides in Fig. 1B.[51,54] The similarity of the EXAFS spectra between the synthesized Mn oxide in this study and reference todorokite supports the formation of todorokite *via* photochemical reaction in the presence of Mg^{2+}. While the combined XRD and EXAFS analyses provide strong evidence for direct todorokite formation, the relatively poor crystallinity indicated by the XRD results, together with the limited dataset derived from *ex situ* analyses at a single reaction time, suggests that minor contributions from other Mn oxide phases, such as birnessite or asbolane, cannot be completely excluded. Future studies employing *in situ* structural characterization can support the assessment of the potential presence of minor Mn oxide phases, including birnessite and asbolane, under environmentally relevant conditions.

Instead of fibrous morphology which occurs from synthesized well-crystalline todorokite through hydrothermal reactions, nucleated todorokite under environmentally relevant system shows a platy morphology (Fig. 1C) that is known for the shape of the poorly crystalline structure of todorokite.[33,55] High resolution transmission electron microscopy (HR-TEM) images of Mn oxides prepared at 100 mM Mg^{2+} at pH 7–8 clearly show *d*-spacings of ~10 Å and ~5 Å occurring from the (001) and (002) basal planes of todorokite, respectively (Fig. 1D).

We note that the observed rapid formation of todorokite nanomaterials is a direct process, resulting from the fast oxidation of Mn^{2+}(aq) by superoxide in the presence of Mg^{2+} under circumneutral pH conditions within 6 h. Although birnessite might occur first and then transform to todorokite in a short time, this scenario is unlikely because the phase transformation is a very slow reaction in the absence of elevated temperatures.[33,34] To transform to todorokite, birnessite must undergo charge redistribution of the Mn(III), but this could occur in a short time only under high temperature conditions.[31] However, even at a high temperature (~90 °C), a 6 h reaction is insufficient to clearly observe this transformation.[33,34] Reported hydrothermal studies show that obtaining substantial evidence of todorokite formation at ~90 °C requires more than 48 h, and that faster transformation rates occur only at higher temperatures, indicating that phase transformation at room temperature is not feasible within 6 h.[33,34] Even nano-sized layer-structured Mn oxides (biogenic Mn oxides) with Mg^{2+} inserted at the interlayer, which might be more feasibly transformed due to their less stable structures, show the phase transformation to todorokite only under hydrothermal temperature conditions (100 °C) for more than 8 h.[33] Thus, under our experimental conditions at room temperature, the observed todorokite was judged to have directly formed from the oxidization of Mn^{2+}(aq) by superoxide within 6 h, rather than through a transformation from a pre-nucleated layered Mn oxide phase.

Of interest, we found that even a small pH difference can change the nanostructure of the Mn oxides. When the same reaction was performed at an initial pH of 6, which is slightly lower than the pH 7–8 at which we observed todorokite, after 6 h reaction with superoxide in the presence of Mg^{2+}, XRD showed only a birnessite-like structure (with basal plane diffractions stronger than those of δ-MnO_2), instead of todorokite (Fig. 1A).

Along with the different mineral nano-phases of the Mn oxides from reactions at pH 7–8 and pH 6, their oxidation states also showed differences. Because Mn 2p is less

sensitive to the bonding environment of Mn oxides and Mn 3s overlaps Mg 1s, we used the highly sensitive Mn 3p peak in analyses of the oxidation state of Mn.[46] X-ray photoelectron spectroscopy (XPS) of Mn 3p clearly shows the difference in the oxidation states of the forms from the two pH conditions (Fig. 2). While Mn(IV) occurs most dominantly under all pH conditions, at pH 7–8, Mn(III) (~33%) is more prevalent than Mn(II) (~8%) (Fig. 2). At pH 6, Mn(II) (~33%) is predominant over Mn(III) (~14%). At pH 6, the inclusion of Mn(II) creates a shoulder peak in the Mn 3p spectra at around 47.8 eV (Fig. 2 and S5). In addition, the shift of the Mn $2p_{3/2}$ peak to lower binding energy at pH 6 compared with pH 7–8 also indicates a greater contribution of Mn(II) at pH 6 (Fig. S6). Taken together, we observed the formation of todorokite containing a substantial fraction of Mn(III) at pH 7–8, whereas δ-MnO_2 formed at pH 6 with a markedly lower Mn(III) content in our system.

Discussion

The significance of Mn(III) in the direct formation of todorokite

The XPS analyses for the Mn oxides formed under varied pH conditions suggest the comproportionation and disproportionation processes of Mn competitively occur depending on pH:

$$\mathrm{Mn(II) + Mn(IV)O_2 + 2H_2O \rightarrow 2Mn(III)OOH + 2H^+} \quad \text{comproportionation} \quad (1)$$

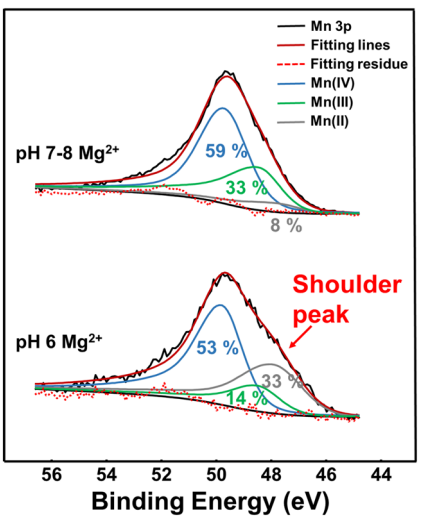

Fig. 2 Predominance of Mn(III) over Mn(II) in Mn oxides prepared at pH 7–8. Although Mn(IV) is the most dominant oxidation state in all reaction systems, analyses of X-ray photoelectron spectroscopy of Mn 3p show that the dominance of Mn(III) or Mn(II) changes depending on the pH condition. The fitting lines of Mn(II), Mn(III), and Mn(IV) are in gray, green, and blue, respectively. At pH 6, a significant extent of Mn(II) occurs at the shoulder peak at around 47.8 eV. This discrepancy in the oxidation state results from the equilibrium of comproportionation–disproportionation reactions, depending on the pH condition.

$$\mathrm{2Mn(III) + 2H_2O \rightarrow Mn(II) + Mn(IV)O_2 + 4H^+} \quad \text{disproportionation} \quad (2)$$

Depending on the equilibrium between eqn (1) and (2), when superoxide oxidizes Mn^{2+}(aq) to Mn(IV), $Mn(IV)O_6$ octahedra can interact with Mn^{2+}(aq) in solution, resulting in comproportionation.[40,41] While the reported equilibrium constants of the reactions vary, depending on the structure of $Mn(IV)O_2$,[40,41,56] based on the reported values and previous experimental results for the reaction,[18,40,41] comproportionation is more likely to dominate over disproportionation when pH is higher than ~7 (Fig. 3). When pH is lower than ~6, the reported studies show that disproportionation occurs dominantly during interactions between $Mn(IV)O_6$ octahedra and Mn^{2+}(aq) in solution.[18,40,41] Thus, the analyses of the structure and oxidation state of Mn oxides in this study show that todorokite nanostructures form at pH 7–8, with a quite significant amount of Mn(III) in the structure, and δ-MnO_2 forms at pH 6 with a much less proportion of Mn(III) than Mn oxides formed at pH 7–8 in the structure.

Previous studies show that the transformation of birnessite to todorokite is driven by Jahn–Teller active Mn(III) under hydrothermal reaction conditions.[31] The transformation of a layered structure to a tunneled structure releases intralayer strain when there is an agglomeration of Jahn–Teller active Mn(III).[8,31,57] Specifically, the release of

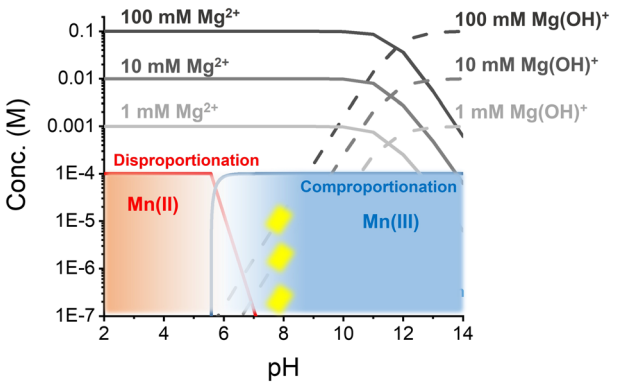

Fig. 3 Thermodynamic equilibrium of disproportionation–comproportionation and Mg^{2+} aqueous species under varied pH conditions. At pH 7–8, the formation of todorokite closely relates to Mn(III), generated from comproportionation, and to aqueous $Mg(OH)^+$ species. The thermodynamic equilibrium of aqueous species in the 1, 10, and 100 mM Mg^{2+}-added solution with 100 μM Mn^{2+}(aq) shows the predominance of Mn(III) and the emerging concentration of $Mg(OH)^+$ at pH 7–8. Yellow bold lines indicate the concentration ranges of $Mg(OH)^+$ at pH 7–8 in the solutions with 1, 10, and 100 mM. Based on the oxidation rates of Mn^{2+}(aq) with superoxide (≤~3.3 μM h^{-1}), the concentration of Mn(III), generated from comproportionation, is comparable to that of $Mg(OH)^+$ in the solutions with 10 and 100 mM Mg^{2+}. The concentrations of $Mg(OH)^+$ in the solutions with 10 and 100 mM Mg^{2+} are orders of magnitude higher than that of $Mg(OH)^+$ in the solution with 1 mM Mg^{2+}. The figure information is generated from thermodynamic calculations using Visual MINTEQ and the thermo.vdh thermodynamic database. The equilibrium concentration of Mn(II) in comproportionation was obtained using an equilibrium constant value of $10^{-7.01}$.

concentrated strain occurs at intralayer pivots, where Mn(III) is agglomerated through the *b* direction of the intralayer.[31] In the hydrothermal transformation of birnessite to todorokite, randomly distributed intralayer Mn(III) in birnessite is re-distributed to intralayer pivot points to release strain under high temperature conditions.[31] However, even at a high temperature (~90 °C), more than 48 h is needed to observe considerable evidence of todorokite formation.[31,33,34] In our room temperature experimental system, such a charge redistribution of Mn(III) is unlikely to occur within a short time (*i.e.*, a few hours). Therefore, we can infer that edge-sharing clusters of $Mn(III)O_6$ octahedra occur, generated from comproportionation. They then interact with other edge-sharing clusters of $Mn(IV)O_6$ octahedra and form an intralayer nanoscale pivot frame.

Role of Mg^{2+} in the direct formation of todorokite under circumneutral conditions

Interestingly, in this nanoscale Mn oxide formation process, we found that Mg^{2+} clearly facilitates the structure formation of todorokite by stabilizing Mn(III), as Hu *et al.* (2018) suggested using the DFT simulation of Mg todorokite structure.[39] To clarify the role of Mg^{2+} in the formation of todorokite, we conducted the photochemical oxidation of Mn^{2+}(aq) in the solution at pH 7–8 by replacing Mg^{2+} with Na^+. In the absence of Mg^{2+}, XRD showed that mainly feitknechtite (β-Mn(III)OOH) formed, in lieu of todorokite (Fig. S7). When we added either 1 or 100 mM Na^+ to the solution at pH 7–8, strong diffractions were observed at ~4.7 and ~2.4 Å (JCPDS 18-804), resulting from the presence of feitknechtite, and weak diffractions from δ-MnO_2 were observed as well. While the results consistently showed evidence of comproportionation at pH 7–8, the absence of todorokite in the presence of Na^+ importantly indicated that the rapid formation of todorokite in solutions was owing to the presence of Mg^{2+}. Moreover, in the presence of Mg^{2+}, a high resolution XPS scan of Mg 1s showed these ions are incorporated in Mn oxides (Fig. S8). On the other hand, for the samples prepared at pH 6, which contained only birnessite (Fig. 1), there were no clearly discernible signals of Mg^{2+} in the high-resolution scan (Fig. S8). In fact, natural todorokite samples include Mg^{2+} in the tunnel, and previous studies of hydrothermal transformation of birnessite to todorokite also show the importance of Mg^{2+}, in framing the large tunnel structure.[31,34,39,58] Although the formation mechanism of todorokite in this study is entirely different from the previously suggested hydrothermal transformation of layer to tunnel structure, the consistent results show the importance of Mg^{2+} in stabilizing the structure of todorokite. In sum, these results indicate that the rapid and direct formation of todorokite *via* the oxidation of Mn^{2+}(aq) by superoxide occurs from Jahn–Teller active Mn(III), generated from comproportionation between Mn(IV) and Mn(II) at pH 7–8, and from the incorporation of Mg^{2+} in the newly forming structure.

It is important to note that the direct homogeneous formation of todorokite from the oxidation of Mn^{2+}(aq) was not observed in biotic processes, which are considered the most effective pathway of the formation of natural Mn oxides.[17,18,27,59] It might be because the studies tested biotic oxidation and formation of Mn oxides in the presence of Na^+ or Ca^{2+}, not Mg^{2+}. Also, the formation of feitknechtite and layered Mn oxides in the presence of Na^+ occurred from this study and previous studies, indicating that the difference in oxidation kinetics and experimental conditions can significantly control the formation of Mn oxides. Under room temperature, Yang *et al.* (2019) tested the transformation of highly adsorbed Mn(II) on layered Mn oxide in the presence of Mg^{2+}.[60] While the study also showed the transformation to triclinic birnessite *via* comproportionation, transformation to todorokite did not occur. The result may also explain the difficulty in the transformation from phyllomanganate to tectomanganate under room temperature, and support that the formation of todorokite occurred directly from the photochemical oxidation of Mn^{2+}(aq) by superoxide in this study. The photocatalytic oxidation of Mn^{2+}(aq) by nucleated todorokite is negligible, as indicated by the similar oxidation rates of Mn^{2+}(aq) between this study (Fig. S9) and our previous study.[21] Under identical experimental conditions (*i.e.*, initial pH 9, 100 μM Mn^{2+}(aq), 1 mM NO_3^-), except for the absence of Mg^{2+}, the previous study showed that the photochemical oxidation of Mn^{2+}(aq) was solely due to superoxide.[21] The similar oxidation rates suggest that the photocatalytic oxidation of Mn^{2+}(aq) by nucleated todorokite can be ruled out.

Stabilization of todorokite through Mn(III)–$Mg(OH)^+$ complexation

To provide insights into the roles of Mn(III) and the complexation of Mg^{2+} in the direct formation of todorokite, we analyzed aqueous species in the solution under different concentrations of Mg^{2+} (Fig. 3). We employed Visual MINTEQ and the 'thermo.vdh' database to calculate the aqueous speciation under varied Mg^{2+} concentrations (1, 10, and 100 mM). At pH 8, the concentrations of $Mg(OH)^+$ aqueous species in the solutions with 1, 10, and 100 mM Mg^{2+} are ~0.3, ~2.5, and ~10.6 μM, respectively. Considering the oxidation rates of Mn^{2+}(aq) to Mn(IV) in this study (≤~3.3 μM h^{-1}) (Fig. S9), the concentrations of $Mg(OH)^+$ species in the solutions with 10 and 100 mM Mg^{2+} were comparable to the amount of oxidized Mn^{2+}(aq). However, in the solution with 1 mM Mg^{2+}, the concentration of $Mg(OH)^+$ species was about one order of magnitude lower (Fig. 3).

Furthermore, the crystalline structure of Mn oxides varied with the concentration of Mg^{2+} in the solutions. Among the solutions with 1, 10, and 100 mM Mg^{2+} at pH 7–8, feitknechtite (β-Mn(III)OOH) was observed only in the solution of 1 mM Mg^{2+}, where the equilibrium concentration of $Mg(OH)^+$ is about one order of magnitude lower than that in the solutions of 10 mM and 100 mM Mg^{2+} (Fig. S10). This

result suggests that the concentration of $Mg(OH)^+$ is an important aqueous species in controlling the formation of todorokite. In such cases, owing to the smaller amount of $Mg(OH)^+$ in the solution of 1 mM Mg^{2+}, only limited Mn oxide precursors can interact with $Mg(OH)^+$ to form todorokite. The remaining Mn(III/IV), which does not interact with $Mg(OH)^+$, develops as feitknechtite likely *via* comproportionation, as confirmed from the test without the addition of Mg^{2+} at pH 7–8 (Fig. S7). While the calculation and structural analyses under the varied concentrations of Mg^{2+} provide an insight into the critical role of $Mg(OH)^+$, future research is warranted to systematically examine the interactions between Mn oxide precursors and soluble Mg species.

Based on the observed Mn oxides, oxidation states, and aqueous species concentrations under the various pH and cation-added conditions, we can infer that Mn(III) interacts with $Mg(OH)^+$, and consequently, $Mg(OH)^+$ is incorporated in the tunnel, framing the large tunnel structure. At pH value above 7, the comproportionation reaction becomes thermodynamically favored over disproportionation (*i.e.*, equilibrium constant (K_{eq}) in eqn (1) is $10^{-7.01}$), and predominates, as demonstrated by previous studies and supported by our calculations (Fig. 3).[40,41] In addition, under these conditions, the concentration of $Mg(OH)^+$ becomes comparable to that of Mn(III), indicating a strong likelihood that $Mg(OH)^+$ stabilizes Mn(III). Phase analysis of Mn oxides formed in the presence and absence of Mg^{2+} further supports the stabilization of todorokite through interactions between edge-sharing Mn(III) octahedra and $Mg(OH)^+$. Moreover, a recent study by Hu *et al.* (2018), using density functional theory (DFT) calculations of the polytypic features ($n \times 3$, where n is an integer referring to the number of edge-sharing MnO_6 octahedron/octahedra in the [100] direction) within todorokite, showed that hydrated Mg ions stabilize todorokite by occupying the tunnel corner site, where they strongly complex with neighboring Mn–O framework.[39] This work offers useful insights into how the edge-sharing clusters of $Mn(III)O_6$ octahedra can be oriented easily in the presence of Mg to the direction of tunnel walls. In addition, Gao *et al.* (2025) employed pair distribution function analysis to determine the location of Mg, supporting the DFT results and validating our hypothesis that Mg occupies tunnel corner sites.[37] Together with TEM measurements of the constrained Mn(III) position in todorokite at the intralayer pivot point,[31] our experimental results and the DFT calculation reported by Hu *et al.* (2018)[39] support the idea that the interaction between Mn(III) and hydrated $Mg(OH)^+$ critically contributes to stabilizing Mn(IV) clusters and framing the large tunnel structure by occupying intralayer pivot points and corner sites of the tunnel, respectively.

In short, the mechanism of the observed rapid and direct formation of todorokite nanostructure can be explained by the occurrence of Mn(III) from comproportionation, by the availability of $Mg(OH)^+$ aqueous species, and by their interactions with Mn oxide precursors, as shown in Fig. 4. Without any ligands that stabilize Mn(III), such as pyrophosphate or siderophore, superoxide oxidizes Mn^{2+}(aq) to Mn(IV) by two-step one-electron transfer.[21,22] Therefore, Mn(III) most likely is formed by comproportionation of adsorbed Mn^{2+}(aq) on $Mn(IV)O_6$ octahedra at pH 7–8 (stage 1 in Fig. 4). This process promotes the formation of edge-sharing clusters of $Mn(III)O_6$ octahedra (stage 2 in Fig. 4). Edge-sharing clusters of Mn(III) and Mn(IV) could interact preferentially with $Mg(OH)^+$ (stage 3 in Fig. 4) to compensate for electron deficiency occurring from Mn(III) in the nanostructure of Mn oxide as the layer-structured Mn oxides accommodate cations in the structure.[39,61] Considering the large size of the hydrated $Mg(OH)^+$ ion,[31,34,39] this structure can act as a framework unit to form todorokite (stages 3 and 4 in Fig. 4). Based on the observed Mn oxides, oxidation states, and aqueous species under various pH and cation-added conditions in this study, it is mechanistically plausible to infer the direct formation of todorokite. Nevertheless, more detailed studies using *in situ* analysis of nucleation and growth at the atomic scale would be helpful to confirm the interaction between Mg^{2+} and Mn(III)/Mn(IV) during direct nucleation of todorokite.

To further test the direct formation of todorokite in a more complicated environmental system, such as ocean, we examined their formation in artificial seawater containing 500 mM Na^+, 50 mM Mg^{2+}, and 10 mM Ca^{2+} at pH 7–8. Fig. 5 shows the formation of todorokite. In other words, $Mg(OH)^+$

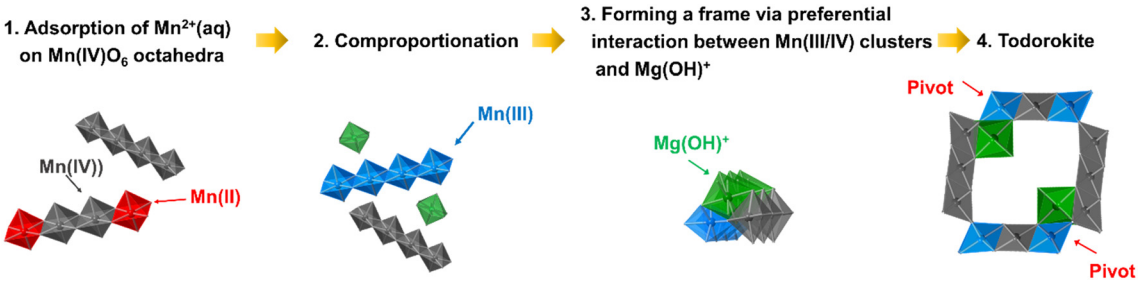

Fig. 4 Schematic illustration of the direct formation mechanism of todorokite *via* the oxidation of Mn^{2+}(aq) with superoxide in the presence of Mg^{2+} under circumneutral conditions. Edge-sharing Mn(III) clusters occur from comproportionation between Mn^{2+}(aq) and $Mn(IV)O_6$ octahedra (stages 1 and 2). Edge-sharing Mn(IV) and Mn(III) clusters in solution interact with $MgOH^+$ and form a framework element of todorokite (stage 3). Further assembly forms todorokite by conforming the frame (stage 4).

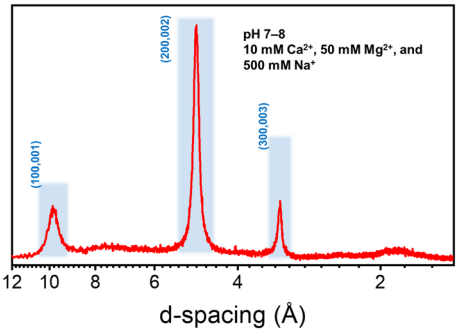

Fig. 5 The formation of todorokite in the presence of multiple cations. Although the concentrations of Mg^{2+} and Ca^{2+} are much lower than that of Na^{+} in the seawater mimicked solution, the XRD result shows the formation of todorokite, suggesting the feasibility of the reaction in environmental systems.

remains active in the formation of todorokite, in competition with the high concentration of Na^{+} that can promote phyllomanganate structure. The resulting todorokite structure can result from the selective interaction between Mn(III) and $Mg(OH)^{+}$. Based on the observed sensitivity of the phase of Mn oxides to pH and cations in this study, the crystalline nanostructure of Mn oxides could indicate the environmental condition when they formed. Because the diverse crystal nanophases of natural Mn oxides are known to depend on the locations where they formed,[62,63] our experimental results can provide a new paradigm for understanding the structural diversity of natural Mn oxides.

Conclusions

Because of the high reduction potential of Mn(IV) oxide/Mn^{2+}(aq) (~500 mV at circumneutral pH), the formation of natural Mn(III/IV) oxide nanomaterials, primarily occurring as layered Mn oxides and todorokite, is crucial for understanding the occurrence, fate and transport of organics and metals in environmental systems.[5,7,64,65] The sorption and redox reactivities of layer- and tunnel-structured nano-Mn oxides are quite distinguishable from each other (*e.g.*, layer-structure Mn oxides have greater oxidative reactivity than tunnel-structure forms).[65,66] Although the reactivities of these structures differ substantially, most studies on the fate and transport of redox-sensitive substances in the environment have focused only on layered Mn oxides. The impact of todorokite on redox reactions in environmental systems has been largely overlooked, likely due to the challenges of elucidating its formation under environmentally relevant conditions. While the biotic and abiotic formations of layer-structured Mn oxide nanomaterials have been deciphered well through extensive studies, todorokite have been considered to form only by the transformation of layer-structured Mn oxides. The evidence from natural Mn oxides supports a transformation-driven occurrence of todorokite, evident in the proportional increase of todorokite compared to birnessite from outer samples (younger precipitates) to inner samples (older precipitates).[67,68] The presence of todorokite in younger precipitates raises the inference of direct todorokite formation, challenging the exclusive reliance on birnessite transformation.[67] Due to the elusive understanding of the accurate formation mechanism, pathway, and kinetics of tunnel-structured Mn oxides to date, the transformation of birnessite has been regarded as the sole pathway for the natural formation of todorokite.[28,29] Here, we show how nanoscale todorokite can occur directly, starting from the oxidation of Mn^{2+}(aq) under environmentally relevant pH and cation conditions at room temperature. Our findings open new research directions for investigating how abiotic and biotic oxidation pathways influence the direct formation of todorokite and for resolving its structural evolution during early-stage formation using real-time analyses.

In addition, todorokite's unique tunnel structure makes it of interest for engineered applications such as catalysts, molecular sieves, and energy storage.[69–71] Our suggested mechanisms are strikingly simpler than the hydrothermal transformation of birnessite to todorokite, which requires many procedures, chemicals, and external energy.[31,34] With further research on the selective formation and optimization of Mn oxides, this research will open a door to the synthesis of various Mn oxides not only by photochemical oxidation but also by another abiotic/biotic oxidation in a sustainable chemistry pathway. This simple and environmentally benign pathway will benefit the synthesis of new materials for environmental catalysts and energy storage applications.[72]

Author contributions

H. J. and Y.-S. J. developed the idea and experiments, and wrote the manuscript. H. J. and Z. G. conducted experiments and analyses. All authors discussed the results, and the manuscript was revised by all authors. Y.-S. J. directed the work.

Conflicts of interest

There are no conflicts to declare.

Data availability

The data supporting this article have been included as part of the supplementary information (SI).

Supplementary information: pH measurement, XPS, XRD, EXAFS, and oxidation kinetics. See DOI: https://doi.org/10.1039/d5en01203a.

Acknowledgements

This work is supported by U.S. National Science Foundation's Environmental Chemical Sciences Program (CHE-1905077). The authors acknowledge Professor James C. Ballard for reviewing the manuscript, and the Environmental NanoChemistry Laboratory Group members for valuable discussions. The authors appreciate the support from the Institute of Materials Science & Engineering (IMSE) of

Washington University in St. Louis for the use of XPS and TEM. H. J. acknowledges the support by the National Research Foundation of Korea (NRF) grant funded by the Korea government (MSIT) (Grant No. RS2025-23525246), and by Global-Learning & Academic research institution for Master's PhD students, and Postdocs (LAMP) Program of the National Research Foundation of Korea (NRF) grant funded by the Ministry of Education (No. RS2024-00444460).

References

1 W. G. Sunda and D. J. Kieber, Oxidation of humic substances by manganese oxides yields low-molecular-weight organic substrates, *Nature*, 1994, **367**, 62–64.
2 T. G. Spiro, J. R. Bargar, G. Sposito and B. M. Tebo, Bacteriogenic manganese oxides, *Acc. Chem. Res.*, 2009, **43**, 2–9.
3 A. S. Madison, B. M. Tebo, A. Mucci, B. Sundby and G. W. Luther, Abundant porewater Mn (III) is a major component of the sedimentary redox system, *Science*, 2013, **341**, 875–878.
4 C. A. Romano, M. Zhou, Y. Song, V. H. Wysocki, A. C. Dohnalkova, L. Kovarik, L. Paša-Tolić and B. M. Tebo, Biogenic manganese oxide nanoparticle formation by a multimeric multicopper oxidase Mnx, *Nat. Commun.*, 2017, **8**, 746–753.
5 M. E. Jones, P. S. Nico, S. Ying, T. Regier, J. Thieme and M. Keiluweit, Manganese-Driven Carbon Oxidation at Oxic–Anoxic Interfaces, *Environ. Sci. Technol.*, 2018, **52**, 12349–12357.
6 H. Li, B. Reinhart, S. Moller and E. Herndon, Effects of C/Mn Ratios on the Sorption and Oxidative Degradation of Small Organic Molecules on Mn-Oxides, *Environ. Sci. Technol.*, 2023, **57**, 741–750.
7 H. Li, F. Santos, K. Butler and E. Herndon, A Critical Review on the Multiple Roles of Manganese in Stabilizing and Destabilizing Soil Organic Matter, *Environ. Sci. Technol.*, 2021, **55**, 12136–12152.
8 H. Jung, M. Taillefert, J. Sun, Q. Wang, O. J. Borkiewicz, P. Liu, L. Yang, S. Chen, H. Chen and Y. Tang, Redox Cycling Driven Transformation of Layered Manganese Oxides to Tunnel Structures, *J. Am. Chem. Soc.*, 2020, **142**, 2506–2513.
9 N. L. Lanza, W. W. Fischer, R. C. Wiens, J. Grotzinger, A. M. Ollila, A. Cousin, R. B. Anderson, B. C. Clark, R. Gellert, N. Mangold, S. Maurice, S. Le Mouélic, M. Nachon, M. Schmidt, J. Berger, S. M. Clegg, O. Forni, C. Hardgrove, N. Melikechi, H. E. Newsom and V. Sautter, High manganese concentrations in rocks at Gale crater, Mars, *Geophys. Res. Lett.*, 2014, **41**, 5755–5763.
10 J. E. Johnson, S. M. Webb, K. Thomas, S. Ono, J. L. Kirschvink and W. W. Fischer, Manganese-oxidizing photosynthesis before the rise of cyanobacteria, *Proc. Natl. Acad. Sci. U. S. A.*, 2013, **110**, 11238–11243.
11 D. Diem and W. Stumm, Is dissolved Mn^{2+} being oxidized by O_2 in absence of Mn-bacteria or surface catalysts?, *Geochim. Cosmochim. Acta*, 1984, **48**, 1571–1573.
12 J. J. Morgan, Kinetics of reaction between O_2 and Mn (II) species in aqueous solutions, *Geochim. Cosmochim. Acta*, 2005, **69**, 35–48.
13 J. J. Morgan, M. A. Schlautman and H. Bilinski, Rates of Abiotic MnII Oxidation by O2: Influence of Various Multidentate Ligands at High pH, *Environ. Sci. Technol.*, 2021, **55**, 14426–14435.
14 P. J. Von Langen, K. S. Johnson, K. H. Coale and V. A. Elrod, Oxidation kinetics of manganese (II) in seawater at nanomolar concentrations, *Geochim. Cosmochim. Acta*, 1997, **61**, 4945–4954.
15 B. Wehrli, G. Friedl and A. Manceau, in *Aquatic Chemistry: Interfacial and Interspecies Processes*, ed. C. P. Huang, C. R. Omelia and J. J. Morgan, American Chemical Society, 1995, vol. 244, pp. 111–134.
16 A. S. Madden and M. F. Hochella, A test of geochemical reactivity as a function of mineral size: Manganese oxidation promoted by hematite nanoparticles, *Geochim. Cosmochim. Acta*, 2005, **69**, 389–398.
17 D. Learman, B. Voelker, A. Vazquez-Rodriguez and C. Hansel, Formation of manganese oxides by bacterially generated superoxide, *Nat. Geosci.*, 2011, **4**, 95–98.
18 M. Zhu, M. Ginder-Vogel, S. J. Parikh, X.-H. Feng and D. L. Sparks, Cation Effects on the Layer Structure of Biogenic Mn-Oxides, *Environ. Sci. Technol.*, 2010, **44**, 4465–4471.
19 B. M. Tebo, Manganese (II) oxidation in the suboxic zone of the Black Sea, *Deep-Sea Res., Part A*, 1991, **38**, S883–S905.
20 P. S. Nico, C. Anastasio and R. J. Zasoski, Rapid photo-oxidation of Mn (II) mediated by humic substances, *Geochim. Cosmochim. Acta*, 2002, **66**, 4047–4056.
21 H. Jung, T. Chadha, D. Kim, P. Biswas and Y.-S. Jun, Photochemically-assisted Fast Abiotic Oxidation of Manganese and Formation of δ–MnO_2 Nanosheets in Nitrate Solution, *Chem. Commun.*, 2017, **53**, 4445–4448.
22 H. Jung, T. S. Chadha, Y. Min, P. Biswas and Y.-S. Jun, Photochemically-assisted Synthesis of Birnessite Nanosheets and Their Structural Alteration in the Presence of Pyrophosphate, *ACS Sustainable Chem. Eng.*, 2017, **5**, 10624–10632.
23 Z. Gao, C. Skurie and Y.-S. Jun, Reactive halogen radicals in saline water promote photochemically-assisted formation of manganese oxide nanosheets, *Environ. Sci.: Nano*, 2022, **9**, 3756–3765.
24 C. D. Georgiou, H. J. Sun, C. P. McKay, K. Grintzalis, I. Papapostolou, D. Zisimopoulos, K. Panagiotidis, G. Zhang, E. Koutsopoulou, G. E. Christidis and I. Margiolaki, Evidence for photochemical production of reactive oxygen species in desert soils, *Nat. Commun.*, 2015, **6**, 7100–7110.
25 J. M. Diaz, C. M. Hansel, B. M. Voelker, C. M. Mendes, P. F. Andeer and T. Zhang, Widespread production of extracellular superoxide by heterotrophic bacteria, *Science*, 2013, **340**, 1223–1226.
26 A. Lu, Y. Li, H. Ding, X. Xu, Y. Li, G. Ren, J. Liang, Y. Liu, H. Hong, N. Chen, S. Chu, F. Liu, Y. Li, H. Wang, C. Ding, C. Wang, Y. Lai, J. Liu, J. Dick, K. Liu and M. F. Hochella, Photoelectric conversion on Earth's surface via widespread

Fe- and Mn-mineral coatings, *Proc. Natl. Acad. Sci. U. S. A.*, 2019, **116**, 9741–9746.

27 D. Learman, S. Wankel, S. Webb, N. Martinez, A. Madden and C. Hansel, Coupled biotic–abiotic Mn (II) oxidation pathway mediates the formation and structural evolution of biogenic Mn oxides, *Geochim. Cosmochim. Acta*, 2011, **75**, 6048–6063.

28 J. E. Post, Manganese oxide minerals: Crystal structures and economic and environmental significance, *Proc. Natl. Acad. Sci. U. S. A.*, 1999, **96**, 3447–3454.

29 P. Yang, S. Lee, J. E. Post, H. Xu, Q. Wang, W. Xu and M. Zhu, Trivalent manganese on vacancies triggers rapid transformation of layered to tunneled manganese oxides (TMOs): Implications for occurrence of TMOs in low-temperature environment, *Geochim. Cosmochim. Acta*, 2018, **240**, 173–190.

30 W. Sun, D. A. Kitchaev, D. Kramer and G. Ceder, Non-equilibrium crystallization pathways of manganese oxides in aqueous solution, *Nat. Commun.*, 2019, **10**, 573.

31 Y. Yuan, K. He, B. W. Byles, C. Liu, K. Amine, J. Lu, E. Pomerantseva and R. Shahbazian-Yassar, Deciphering the Atomic Patterns Leading to MnO2 Polymorphism, *Chem*, 2019, **5**, 1793–1805.

32 D. Golden, C. Chen and J. Dixon, Synthesis of todorokite, *Science*, 1986, **231**, 717–719.

33 X. H. Feng, M. Zhu, M. Ginder-Vogel, C. Ni, S. J. Parikh and D. L. Sparks, Formation of nano-crystalline todorokite from biogenic Mn oxides, *Geochim. Cosmochim. Acta*, 2010, **74**, 3232–3245.

34 X. Feng, H. Zhao, F. Liu, H. Cui, W. Tan and W. Li, in *Advances in the Environmental Biogeochemistry of Manganese Oxides*, American Chemical Society, 2015, ch. 6, vol. 1197, pp. 107–134.

35 J. Heo and H. Jung, Tailoring Oxidation State of Manganese Enables the Direct Formation of Todorokite, *ACS Nano*, 2025, **19**, 12910–12919.

36 H. Jung, C. Snyder, W. Xu, K. Wen, M. Zhu, Y. Li, A. Lu and Y. Tang, Photocatalytic Oxidation of Dissolved Mn2+ by TiO2 and the Formation of Tunnel Structured Manganese Oxides, *ACS Earth Space Chem.*, 2021, **5**, 2105–2114.

37 Z. Gao, H. Jung, O. J. Borkiewicz, K. M. Wiaderek and Y.-S. Jun, Roles of surface Mn(III) and $MgOH^+$/$CaOH^+$ complexation in photochemically assisted Mn^{2+} oxidation and Todorokite formation, *Chem. Eng. J.*, 2025, **519**, 165252.

38 Y. Shen, R. Zerger, R. DeGuzman, S. Suib, L. McCurdy, D. Potter and C. O'young, Manganese oxide octahedral molecular sieves: preparation, characterization, and applications, *Science*, 1993, **260**, 511–515.

39 X. Hu, D. A. Kitchaev, L. Wu, B. Zhang, Q. Meng, A. S. Poyraz, A. C. Marschilok, E. S. Takeuchi, K. J. Takeuchi, G. Ceder and Y. Zhu, Revealing and Rationalizing the Rich Polytypism of Todorokite MnO2, *J. Am. Chem. Soc.*, 2018, **140**, 6961–6968.

40 E. J. Elzinga, Reductive Transformation of Birnessite by Aqueous Mn(II), *Environ. Sci. Technol.*, 2011, **45**, 6366–6372.

41 J. P. Lefkowitz, A. A. Rouff and E. J. Elzinga, Influence of pH on the Reductive Transformation of Birnessite by Aqueous Mn(II), *Environ. Sci. Technol.*, 2013, **47**, 10364–10371.

42 H. Jung, B. Lee, D. Kim, Z. Gao, P.-I. Chou and Y.-S. Jun, Three Distinctive Steps for Heterogeneous Nucleation of Tunnel-Structured Mn Oxide on Quartz under Light Exposure, *Environ. Sci. Technol.*, 2024, **58**, 21200–21209.

43 Z. Gao, D. Zhang and Y.-S. Jun, Does Tert-Butyl Alcohol Really Terminate the Oxidative Activity of ·OH in Inorganic Redox Chemistry?, *Environ. Sci. Technol.*, 2021, **55**, 10442–10450.

44 Z. Gao, P.-I. Chou, B. Lee, Y. Zhu, D. Ghim and Y.-S. Jun, Effects of Sodium and Magnesium Ions on the Photochemically Induced Heterogeneous Formation of Manganese Oxides and Their Structural Evolution, *J. Phys. Chem. C*, 2023, **127**, 12558–12567.

45 B. M. Tebo, B. G. Clement and G. J. Dick, Biotransformations of manganese, Manual of, *Environ. Microbiol.*, 2007, **3**, 1223–1238.

46 E. S. Ilton, J. E. Post, P. J. Heaney, F. T. Ling and S. N. Kerisit, XPS Determination of Mn Oxidation States in Mn (Hydr) oxides, *Appl. Surf. Sci.*, 2016, **366**, 475–485.

47 K. M. Sutherland, S. D. Wankel, J. R. Hein and C. M. Hansel, Spectroscopic Insights Into Ferromanganese Crust Formation and Diagenesis, *Geochem. Geophys. Geosyst.*, 2020, **21**, e2020GC009074.

48 D. C. Golden, J. B. Dixon and C. C. Chen, Ion Exchange, Thermal Transformations, and Oxidizing Properties of Birnessite, *Clays Clay Miner.*, 1986, **34**, 511–520.

49 S. Webb, B. Tebo and J. Bargar, Structural characterization of biogenic Mn oxides produced in seawater by the marine Bacillus sp. strain SG-1, *Am. Mineral.*, 2005, **90**, 1342–1357.

50 Z. Wu, B. Lanson, X. Feng, H. Yin, Z. Qin, X. Wang, W. Tan, Z. Chen, W. Wen and F. Liu, Transformation of Ni-containing birnessite to tectomanganate: Influence and fate of weakly bound Ni(II) species, *Geochim. Cosmochim. Acta*, 2020, **271**, 96–115.

51 S. Webb, C. Fuller, B. Tebo and J. Bargar, Determination of uranyl incorporation into biogenic manganese oxides using X-ray absorption spectroscopy and scattering, *Environ. Sci. Technol.*, 2006, **40**, 771–777.

52 A. L. Atkins, S. Shaw and C. L. Peacock, Release of Ni from birnessite during transformation of birnessite to todorokite: Implications for Ni cycling in marine sediments, *Geochim. Cosmochim. Acta*, 2016, **189**, 158–183.

53 S. Bodeï, A. Manceau, N. Geoffroy, A. Baronnet and M. Buatier, Formation of todorokite from vernadite in Ni-rich hemipelagic sediments, *Geochim. Cosmochim. Acta*, 2007, **71**, 5698–5716.

54 D. A. McKeown and J. E. Post, Characterization of manganese oxide mineralogy in rock varnish and dendrites using X-ray absorption spectroscopy, *Am. Mineral.*, 2001, **86**, 701–713.

55 S. Turner and P. R. Buseck, Todorokites: A New Family of Naturally Occurring Manganese Oxides, *Science*, 1981, **212**, 1024–1027.

56 J. K. Klewicki and J. J. Morgan, Kinetic Behavior of Mn(III) Complexes of Pyrophosphate, EDTA, and Citrate, *Environ. Sci. Technol.*, 1998, **32**, 2916–2922.
57 Y.-F. Li, S.-C. Zhu and Z.-P. Liu, Reaction network of layer-to-tunnel transition of MnO_2, *J. Am. Chem. Soc.*, 2016, **138**, 5371–5379.
58 B.-R. Chen, W. Sun, D. A. Kitchaev, J. S. Mangum, V. Thampy, L. M. Garten, D. S. Ginley, B. P. Gorman, K. H. Stone, G. Ceder, M. F. Toney and L. T. Schelhas, Understanding crystallization pathways leading to manganese oxide polymorph formation, *Nat. Commun.*, 2018, **9**, 2553–2561.
59 S. M. Webb, B. Tebo and J. Barger, Structural influences of sodium and calcium ions on the biogenic manganese oxides produced by the marine Bacillus sp., strain SG-1, *Geomicrobiol. J.*, 2005, **22**, 181–193.
60 P. Yang, J. E. Post, Q. Wang, W. Xu, R. Geiss, P. R. McCurdy and M. Zhu, Metal Adsorption Controls Stability of Layered Manganese Oxides, *Environ. Sci. Technol.*, 2019, **53**, 7453–7462.
61 B. Lanson, V. A. Drits, Q. Feng and A. Manceau, Structure of synthetic Na-birnessite: Evidence for a triclinic one-layer unit cell, *Am. Mineral.*, 2002, **87**, 1662–1671.
62 R. M. Potter and G. R. Rossman, The manganese-and iron-oxide mineralogy of desert varnish, *Chem. Geol.*, 1979, **25**, 79–94.
63 R. M. Potter and G. R. Rossman, Mineralogy of manganese dendrites and coatings, *Am. Mineral.*, 1979, **64**, 1219–1226.
64 E. L. Trainer, M. Ginder-Vogel and C. K. Remucal, Selective Reactivity and Oxidation of Dissolved Organic Matter by Manganese Oxides, *Environ. Sci. Technol.*, 2021, **55**, 12084–12094.
65 C. K. Remucal and M. Ginder-Vogel, A critical review of the reactivity of manganese oxides with organic contaminants, *Environ. Sci.: Processes Impacts*, 2014, **16**, 1247–1266.
66 J. Huang, S. Zhong, Y. Dai, C.-C. Liu and H. J. Zhang, Effect of MnO_2 phase structure on the oxidative reactivity toward contaminant degradation, *Environ. Sci. Technol.*, 2018, **52**, 11309–11318.
67 S. Lee and H. Xu, XRD and TEM studies on nanophase manganese oxides in freshwater ferromanganese nodules from Green Bay, Lake Michigan, *Clays Clay Miner.*, 2016, **64**, 523–536.
68 H. Xu, T. Chen and H. Konishi, HRTEM investigation of trilling todorokite and nano-phase Mn-oxides in manganese dendrites, *Am. Mineral.*, 2010, **95**, 556–562.
69 N. Kumagai, S. Komaba, K. Abe and H. Yashiro, Synthesis of metal-doped todorokite-type MnO2 and its cathode characteristics for rechargeable lithium batteries, *J. Power Sources*, 2005, **146**, 310–314.
70 J. Pakarinen, R. Koivula, M. Laatikainen, K. Laatikainen, E. Paatero and R. Harjula, Nanoporous manganese oxides as environmental protective materials—Effect of Ca and Mg on metals sorption, *J. Hazard. Mater.*, 2010, **180**, 234–240.
71 Z.-R. Tian, W. Tong, J.-Y. Wang, N.-G. Duan, V. V. Krishnan and S. L. Suib, Manganese Oxide Mesoporous Structures: Mixed-Valent Semiconducting Catalysts, *Science*, 1997, **276**, 926–930.
72 Z. Gao, M. Song, Y. Wang, L. M. Santino, J. M. D'Arcy and Y.-S. Jun, Photochemically Assisted Formation of Layered Manganese Oxide Nanosheets with High Pseudocapacitance for Potential Environmental Applications, *ACS Appl. Mater. Interfaces*, 2025, **17**, 56054–56063.